Proceedings of the 26th International Conference on
Port and Ocean Engineering under Arctic Conditions
June 14-18, 2021, Moscow, Russia

Numerical Simulation of Ship Ramming in Extremely Thick Ice

Junji SAWAMURA
Department of Naval Architecture and Ocean Engineering, Osaka University, Osaka, Japan

ABSTRACT

This paper proposes a 2D numerical model for calculating ship ramming in extremely thick plate ice. The calculations include ship–ice collision, ship slide-up onto ice, and icebreaking. The ship–ice collision and ship slide-up calculation are performed using a 2D physically-based model. Ship motions are described using a three-degree-of-freedom equation of motion. The ship–ice collisions are represented using a contact detection algorithm. The collision response is calculated using an instantaneous impulse. The bending failure of plate ice is applied for a criterion of ramming icebreaking. A buoyancy and drag force are included for the fluid force acting on the broken ice floes. The calculated results are compared with the measured data collected when an icebreaker encountered multi-year ice. The icebreaking mechanism of ship ramming is discussed using the measured and numerical results.

KEY WORDS: Ship ramming; Multi-year ice; Icebreaker; Numerical modeling

INTRODUCTION

When an icebreaker encounters thick ice, ramming icebreaking is involved instead of continuous icebreaking. Ramming icebreaking requires specific ship handling that reiterates ship acceleration, collisions with an ice edge, sliding up plate ice, icebreaking, and returning to the start point after icebreaking. A large impact force and ship motions are generated by ship–ice collision and ship slide-up during ship ramming. Ship handling during ramming is difficult and requires a lot of engine power. Understanding a ship's response during ship ramming and predicting ship ramming performance are required for safe and efficient ramming operation.

To calculate ship ramming, ship–ice collision, ship slide-up, and icebreaking can be represented analytically or theoretically. Popov et al., (Dalay et al., 1990) conducted an earlier study on ship ramming using a theoretical approach. They assumed that ship–ice interactions during ship ramming were a ship–ice impact problem and used the energy conservation to derive a simple formula for calculating ramming force. The icebreaking of ship ramming is divided into two parts: the initial impulse and beaching phase. Vaughan (1986) analyzed the flexural response of icebreaking to an impact force using an analytical approach. He calculated the effect of the ship flexure using the maximum bending moment during ship ramming. Blanchet et al., (1990) used the principle of energy conservation to represent ice behavior during ship ramming. Six local energies are described by the theoretical derivations: bending, cracking, flaking, crushing, ship/ice frictional and removal energies. The most important local ice and global ship energies were calculated. Kishi et al., (1997) used an energy balance model to predict the penetration distance of ship ramming

using measured data and model test data. Ringsberg et al., (2014) analyzed the relation between the measured ship motions and ice loads. They proposed a computational model to identify ramming force during ship–ice events in heavy ice conditions. Sawamura et al., (2020) calculated ramming distance using an energy conservation model proposed by Vinogradov (Nozawa, 2006). The calculated ramming penetration distance was compared with measured data. Several papers on ship ramming have been published. However, most of the proposed methods on ship ramming are developed using measured and/or experimental data. A more comprehensive method is needed to predict ship ramming performance.

This paper proposes a 2D numerical model to calculate icebreaking during ship ramming in extremely thick ice. The calculation includes ship–ice collision, ship slide-up, and icebreaking of plate ice. Ship–ice collision and ship slide-up are calculated using 2D physically-based modeling. Ship motions are described using a three-degree-of-freedom (3DOF) equation of motion. Ship–ice collisions are represented using a contact detection algorithm. Collision response is calculated using an instantaneous impulse. A bending failure of plate ice is applied to a criterion of ramming icebreaking. A buoyancy and drag force are included for the fluid force acting on broken ice floes. The calculation results are compared with the measured data when an icebreaker encounters multi-year ice. The icebreaking mechanism of ship ramming was discussed using measured and numerical results.

MEASURED SHIP RAMMING

Japanese icebreaker Shirase II often encounters multi-year ice during her Antarctic voyage. Shirase II is equipped with a ship-monitoring system that records ship motion data during voyage (Yamauch et al., 2011). The data recorded during the 55th Japanese Antarctic Research Expedition (JARE 55) between December 2013 and March 2014 are used in this study. During the outbound voyage to Japanese research station (Showa), Shirase II started her ramming operations from December 18, 2013, when she entered multi-year ice (69°00'N, 39°05'E), and continued until January 4, 2014, when she berthed at Showa station (69°00'N, 39°38'E). This paper used ramming icebreaking data from January 1-January 4, 2014, ramming operation. Figure 1 shows the shipping route of the Shirase II in the multi-year ice and specify the calculated sea ice area.

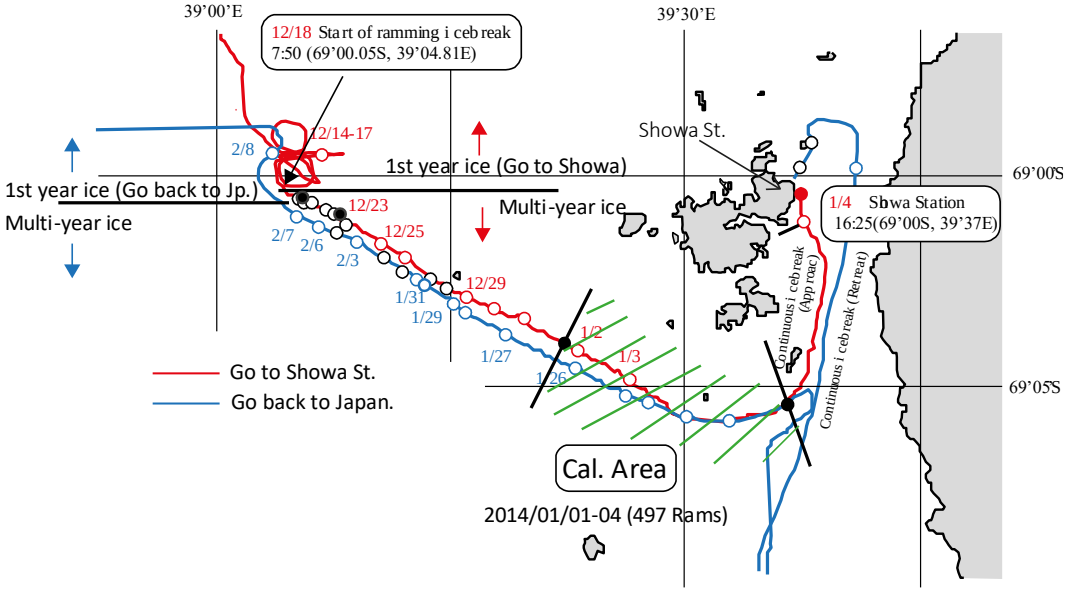

Figure 1. The shipping route of the Shirase II in multi-year ice and the calculated sea ice area

The ship's speed, motion (pitch and roll angle), and thrust with a time interval of 0.01 s are recorded by the ship-monitoring system (Sawamura et al., 2020). Ice thickness was measured using an electromagnetic induction sensor (EM sensor) installed at the starboard shoulder. The EM sensor measures the total sea ice thickness (snow + ice). The time interval of the EM sensor is 1.0 s. Figure 2 shows the measured penetration distance and sea ice thickness. The penetration distance of ramming is defined as the distance between the arrival points of a present and a previous ram. The measured penetration distance gradually increases as sea ice thickness decreases. The distance is greater than 100 m when the ice thickness is below 3.0 m. Figures 3 and 4 show the time history of the ship's motion during one cycle of ship ramming. In Figures 3 and 4, the pitch motion in the bow-up direction expresses a negative value. The ship accelerates at approximately 10 kt ship speed and collides with an ice edge. The ship's speed is rapidly decreased by the ship–ice collision. At the same time, the pitch angle rapidly increases quickly as the ship slides up the ice. The roll angle varies not only during the ship–ice collision and sliding phase but also during acceleration. The ship's maximum pitch angle when ramming into an ice thickness of 3 m (Figure 3) is less than an ice thickness of 5 m (Figure4). The pitch angle during ramming depends on ice thickness.

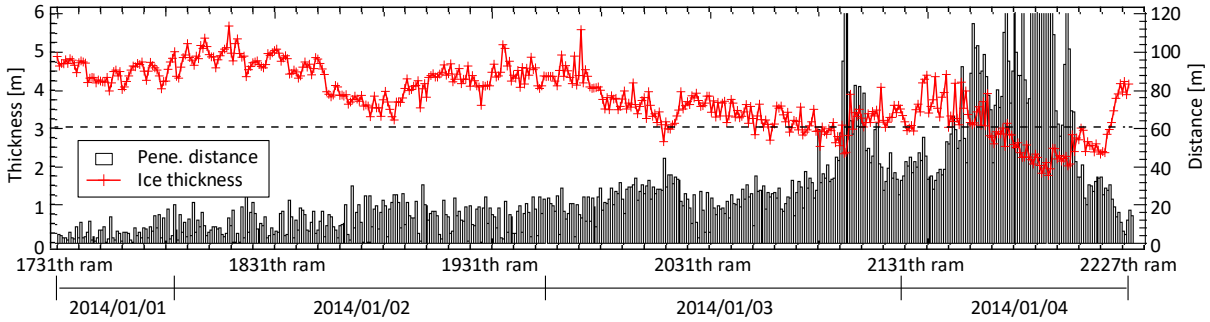

Figure 2. Measured penetration distance and ice thickness on Jan.1 and 4, 2014

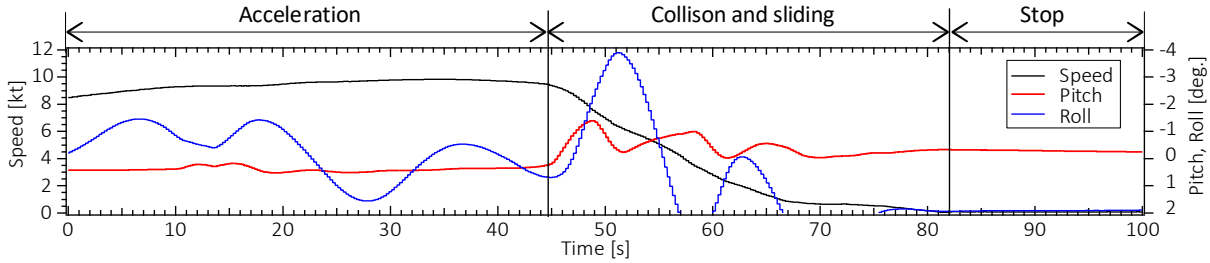

Figure 3. The time history of the measured ship's motion (speed, pitch, and roll angle) during ramming (Ice thickness = 3.02 m, Penetration = 57.23 m, and Location = –69.09 N, 39.48 E)

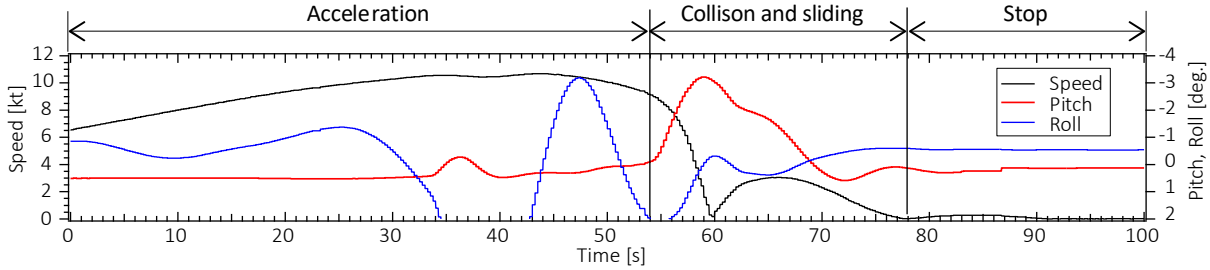

Figure 4. The time history of the measured ship's motion (speed, pitch, and roll angle) during ramming (Ice thickness = 5.07 m, Penetration = 5.52 m, and Location = –69.06 N, 39.31 E)

NUMERICAL MODELING OF SHIP RAMMING

Ice Edge Crushing and Ice Bending Failure

Sawamura et al. (2009) developed a 2D numerical model to predict the ice force experienced by an icebreaker as it advances through plate ice. The numerical model proposed by Sawamura et al. (2009) focused on icebreaking at the waterline. The rotation and sliding of broken ices underwater hull were neglected. This paper includes ship–ice interactions underneath the waterline of broken ices in the proposed numerical model. This numerical model divides ship–ice interactions into three parts: ship–ice contacts, bending failure of plate ice, and ship–ice interaction of broken ice floes.

A circle contact detection technique (e.g., Dimgliana et al., 2000) is used to identify the contact point between a ship hull and an ice edge. Small contact circles are arranged on the ship's hull and the outer surface of the ice. The distance between ship's contact circles and the ice's contact circles is calculated at each time step of the calculation. When two bodies (ship and ice) collide, the distance between their contact circles becomes zero. Figure 5 (a) presents a schematic of circle contact detection applied to ship–ice contacts.

At the ship–ice contact, the ice edge is crushed as the ship advances. Assuming that the ice pressure on the crushing surface is constant, the force induced due to ice crushing is

$$F_{\mathrm{nom}} = A_{\mathrm{c}}\sigma_{\mathrm{c}} \ , \tag{1}$$

where A_{c} represents the crushed area due to the ship–ice contact and σ_{c} denotes the compressive strength of ice. F_{nom} acts in the direction normal to the ice-crushing surface. In the numerical calculation, crushed area A_{c} is calculated using the sum of the ice contact circles on the contact surface between the ship hull and ice.

Kinematic friction is considered in a direction horizontal to the ice-crushing surface. Coulomb-type friction is represented as

$$F_{\mathrm{fric}} = f_i F_{\mathrm{nom}} \ , \tag{2}$$

where f_{i} denotes the friction coefficient between the ship and ice. The direction of the frictional force is opposite to the relative velocity between the ship and ice.

The total ice force attributable to ship–ice interaction is calculated using the sum of the contact force F_{nom} and friction force F_{fric}. The total ice force is divided into vertical and horizontal components at the contact surface, and is derived as the following equations

$$F_{\mathrm{z}} = A_{\mathrm{c}}\sigma_{\mathrm{c}}(\sin\theta - f_i\cos\theta),\ F_{\mathrm{x}} = A_{\mathrm{c}}\sigma_{\mathrm{c}}(\cos\theta + f_i\cos\theta), \tag{3}$$

where θ denotes the ship hull angle. For simplicity, hydrodynamic forces induced by the ship motion and water effects of the floating plate-ice are neglected during the plate ice breaking. The schematics of the crushed area A_{c}, direction of the contact force F_{nom} and the friction force F_{fric} are shown in Figure 5 (b).

Bending failure of plate ice occurs when the contact force F_{z} at the crushing surface A_{c} increases as the ship advances and exceeds the bearing force of plate ice. The bearing force proposed by Kashteljan (Nozawa, 2006) is used.

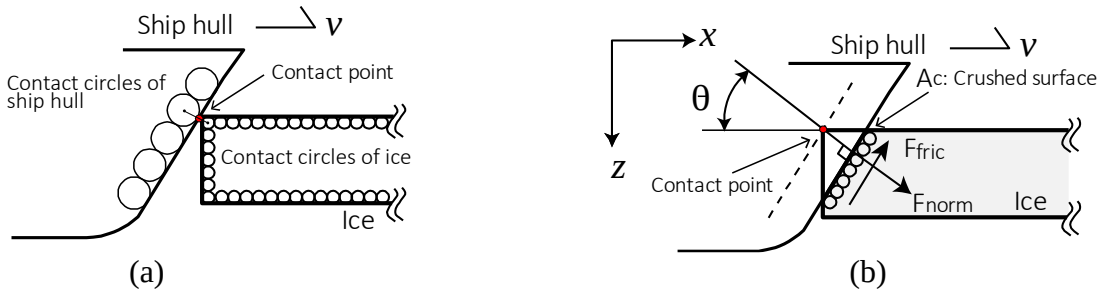

Figure 5. Ship–ice interactions during icebreaking, (a) Circle contact detection, (b) Crushed area, contact force and friction force on the contact surface

$$P = 0.518\sigma_f h^2 \ , \tag{4}$$

where σ_f denotes the flexural strength of ice. h represents the thickness of the plate ice. The length of a broken ice floe is obtained from the theoretical solution of 2D beam theory. For a 2D semi-infinite elastic founding beam with an edge load, the maximum point (breaking length) of the bending stress is

$$x = \frac{\pi}{4}\sqrt{2}l_c \ , \ l_c = \sqrt[4]{\frac{Eh^3}{12\rho_w g}} \ , \tag{5}$$

where l_c denotes the characteristic length of ice. E represents young's modulus of ice. ρ_w denotes the water density. g is the gravitational acceleration. When a plate ice is broken by a ship ramming, the ice within the breaking length is removed from the plate ice, which is defined as the broken ice floe after the ice failure.

Ship and Ice Floe Motion

Physically-based modeling (e.g., Baraff, 1997) is used to calculate ship motions and broken ice floes. The ship and ice floes are assumed to be rigid bodies. Ship motions and the ice floes are described using a 3DOF rigid body equation. The position and rotation of the ship and ice floes are solved using Newton's second law. The repetitive ship–ice and ice–ice contacts of the broken ice floe are represented using a circle contact detection algorithm which is the same as the calculation of ship and plate ice contacts (see Figure 5 (a)). The collision response between two objects (e.g., ship–ice and ice–ice of broken ice floe) is calculated using an instantaneous impulse. Impulse vector **J** in a normal direction at the contact surface can be expressed as

$$\mathbf{J} = j \cdot \mathrm{n}_{ik} \ , \ = \frac{-(1+\varepsilon)v_{\mathrm{ref}}}{\frac{1}{m_i}+\frac{1}{m_k}+\mathbf{n}_{ik}\left\{\left(\mathbf{I}_i^{-1}(\mathbf{r}_i \times \mathbf{n}_{ik})\times \mathbf{r}_k + \left(\mathbf{I}_k^{-1}(\mathbf{r}_k \times \mathbf{n}_{ik})\times \mathbf{r}_i\right)\right)\right\}} \ , \tag{6}$$

where j is the magnitude of an impulse;, $\mathbf{n}_{ik}$ is the direction of an impulse force of an object i received from an object k;, ε is a coefficient of restitution;, v_{ref} is the relative velocity between the two objects;, m_i is the mass of the object i;, and $\mathbf{I}_i$ is the inertia of the object i;, and r_i is the displacement vector representing a displacement from the center of mass of the object i to the center of a contact circle. The time interval of an impulsive response is assumed to be 0.0005

s, which is used to convert impulsive force [Ns] to peak force [N]. A mechanical friction force of the Coulomb model is presented in the horizontal direction to the collision surface. A fluid force of the surrounding water acting on an ice floe is represented by

$$\boldsymbol{F}_{\mathrm{w}} = -\mathrm{C_D} A \frac{1}{2} \rho_w |\boldsymbol{v}| \boldsymbol{v} \ , \tag{7}$$

where C_D is the drag coefficient, A is a projected area and $\boldsymbol{v}$ is the velocity vector of an ice floe. The direction of the fluid force is opposite to the motion of the ice floe. The drag coefficient C_D is assumed to be 0.5. For simplicity, other fluid forces related to ship motions are neglected.

COMPARISON OF SHIP RAMMING

Calculation Conditions

Numerical results of the proposed model are compared with the ship ramming data collected when Japanese icebreaker Shirase II encountered multi-year ice during her Antarctic voyage in 2014 January (JARE 55). The measured ship's speed, thrust, and ice thickness were used for calculations. The measured maximum speed and thrust during ramming were used as input data for calculations. The mechanical properties of sea ice were not measured in JARE 55. The flexural strength estimated using an empirical formula based on the brine volume of sea ice that was measured in JARE 51 (Dec. 2009 - Mar. 2010) was used. The coefficient of restitution obtained from collision tests with a pure ice block and ice sphere is available (Araoka and others, 1978). Young's modulus, compression strength, and coefficient of friction of ice converted from the model ship size to the real ship size in the model test conducted by Japan Marine United Corp. (JMU Corp.) are selected (Sawamura et al., 2017). The reason is the flexural strength used in the model test in JMU Corp. (σ_f = 494 kPa) has values similar to those in JARE 51 (σ_f = 498 kPa). However, the ice thickness used in the model test was 1.5 m (level ice), but 3 – 4 m in JARE 51 (multi-year ice). The mechanical properties of sea ice may be different between the level ice and multi-year ice. The penetration distance in the ship ramming strongly is affected by the mechanical properties. The detailed investigation of the effects of the material properties on the penetration distance (e.g. sensitive analysis using the in-situ measurement data of the sea ice) should be done in the future work. The principal dimensions of the icebreaker Shirase II and the mechanical properties of sea ice are shown, respectively, in Tables 1 and 2. The density of ice and water were 916 kg/m^3 and 1010 kg/m^3, respectively. The gravitational acceleration was 9.8 m/s^2. The ship collides with the ice edge at an initial speed, and moves with a 3DOF rigid body motion and the constant thrust after colliding with the ice. The time interval of the calculations was 0.0005 s.

Table 1. The principal dimension of Japanese icebreaker Shirase II

Length of water line	126.0 m
Maximum breadth	28.0 m
Design draft	9.2 m
Bow angle	19 deg.
Maximum displacement	approx. 20,000 t

Table 2. Mechanical properties of ice

Young's modulus	E	300 MPa
Flexural strength	σ_f	0.5 MPa
Compression strength	σ_c	0.7 MPa
Coefficient of friction		0.1
Coefficient of restitution		0.7

Table 3. Measured ship ramming

Ice thickness Min. - Max. (The number of ramming)	Penetration distance [m]	Maximum Pitch [deg.]	Maximum speed [kt]	Maximum thrust [kN]	Thickness [m]
	Upper: Avg. Lower: SD	Upper: Avg. Lower: SD	Upper: Avg. Lower: SD	Upper: Avg. Lower: SD	Upper: Avg. Lower: SD
1.8 – 3.0 m (78 Rams.)	82.35 (79.33)	1.03 (0.40)	10.37 (0.67)	1202 (38)	2.56 (0.32)
3.0 – 3.5 m (88 Rams.)	41.90 (25.86)	1.57 (0.49)	10.57 (0.62)	1214 (58)	3.25 (0.15)
3.5 – 4.0 m (94 Rams.)	22.82 (15.79)	1.99 (0.53)	10.85 (0.71)	1248 (81)	3.73 (0.14)
4.0 – 4.5 m (103 Rams.)	13.53 (11.51)	2.31 (0.54)	10.65 (0.97)	1288 (91)	4.26 (0.14)
4.5 – 5.0 m (80 Rams.)	10.04 (6.52)	2.60 (0.45)	10.69 (0.93)	1338 (154)	4.73 (0.13)
5.0 – 5.7 m (16 Rams.)	9.64 (6.45)	2.70 (0.58)	11.04 (0.32)	1427 (73)	5.20 (0.19)

Penetration Distance of Ship Ramming

The calculated penetration distance of ship ramming was compared with the measured one. Table 3 shows the measured penetration distance, maximum pitch angle, ship speed, and thrust during one cycle of ship ramming. The averaged values of the maximum pitch, speed, and thrust of the ship rams in each ice thickness are shown. The penetration distance decreases as ice thickness increases, but the pitch angle increases as ice thickness increases. The ship's speed and thrust increase slightly with an increase in ice thickness. The calculation is conducted with constant thrust during the one cycle of ship ramming.

Figure 6 shows the calculated ship ramming. The ice thickness was 4.5 m. The ship's initial speed was 5.0 m/s. The constant thrust given at the center of gravity of the ship is 40 kN/m. Figure 7 shows the calculated time history of the ship's speed and pitch angle during one cycle of ship ramming. The ship speed in Figure 7 shows on the absolute value. Figure 8 shows the calculated ice force acting on the ship hull during ship ramming. The ship collides with the ice edge at 1.4 s, and the ice edge is crushed by the ship advancing. The ice contact force rapidly increases as the crushing area increases (the first peak force in Figure 8). The ice bending failure occurs at 1.7 s. The ice within the breaking length is removed from the plate ice. The broken ice floe rotates and collides with ship hull at 4.0 s, which induces the spike force (the second peak force) as shown in Figure 8. The second collision with the plate

ice occurs at 5.7 s; at the same time, the ship slides up the plate ice. The ship contact force increases as the crushing area increases, but the ice bending failure does not occur after the second ship–ice collision. The ship slides down from the plate ice and finally advances backward. During ship rumming, the contact force F_{nom} is larger than the friction force F_{fric} in the ship-ice interactions of both plate ice and broken ice floes.

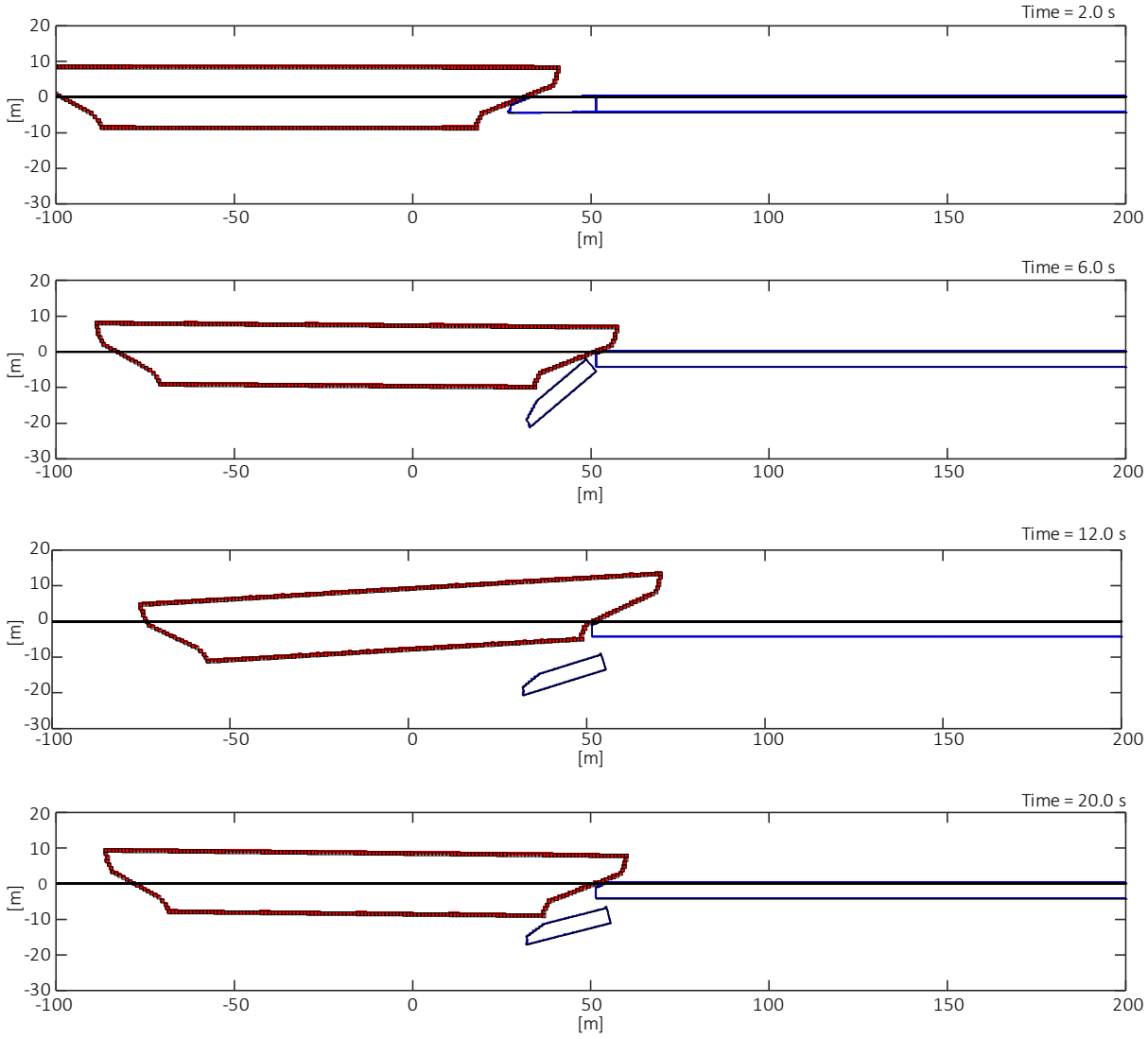

Figure 6. Calculated ship ramming (Ice thickness = 4.5 m, Penetration distance = 22.84 m, Ramming No. 04 in Table 4)

Table 4 shows the calculated penetration distance, maximum pitch angle during one cycle of ship ramming, and input thrust. In all calculations, the initial ship speed of 5.0 m/s (approximately 10 kt) was used. A constant thrust was used in one cycle of the ramming. The calculated penetration distance was slightly shorter than the measured ones, but there was good agreement across all ice thickness. The calculated pitch angles were larger than the measured one in all ice thicknesses. This reason is because the calculation does not account for the effect of flexural deformations in both the ship's longitudinal hull and plate ice. Moreover, the penetration distance is strongly affected by ice's surface conditions such as

snow and ice melted water. Snow has a cushioning effect on the penetration distance, and ice melt water reduces the friction between the ship hull and ice and elongates the ramming distance. The calculations did not consider the effects of snow and ice melt water. Furthermore, even during one cycle of ship ramming, the ice thickness and mechanical properties of real sea ice are not constant. These effects should be researched and accounted for in the calculation.

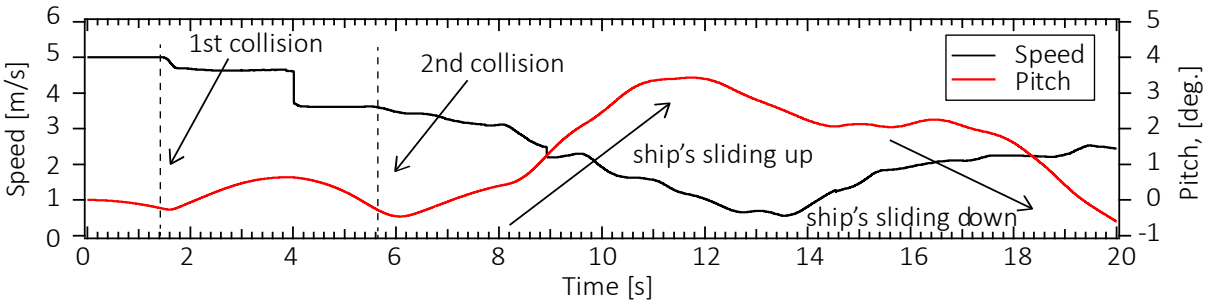

Figure 7. The time history of the calculated ship speed and pitch during ship ramming (Ice thickness = 4.5 m, Penetration distance = 22.84 m, Ramming No. 4 in Table 4)

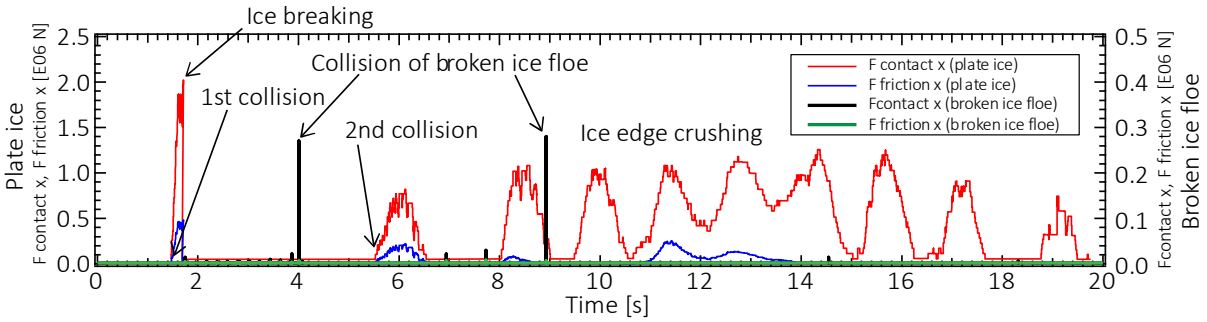

Figure 8. The time history of the calculated ice force (contact force and friction force) in the *x*-direction during ship ramming (Ice thickness = 4.5 m, Penetration distance = 22.84 m, Ramming No. 4 in Table 4)

CONCLUSIONS8

This paper proposes a 2D numerical model to simulate the ship ramming through extremely thick ice. The calculated penetration distance and pitch angle are compared with the measured data by the icebreaker Shirase II during the 55th Japanese Antarctic Research Expedition in 2014. The calculated penetration distance agrees well with the measured ones. However, the calculations produced a larger pith angle than the actual sea measurement. The numerical model does not consider the flexural deformation of the ship and plate ice, the effect of snow and ice melt water on ice surfaces, the distributions of the mechanical properties of sea ice. These effects should be included in calculations in future work.

ACKNOWLEDGEMENTS

The authors would like to thank members of the 55th Japanese Antarctic Research Expedition and crew of Japanese icebreaker Shirase II for the great support in field tests and measurements in Antarctic sea ice. We also acknowledge the Antarctic Research Support Section, Ministry of Defense, for their permission to publish this work. This work was partially supported by the National Institute of Polar Research (NIPR) through General Collaboration Project no. 31-18 and the Arctic Challenge for Sustainability II (ArCS II), Program Grant Number JPMXD1420318865.

Table 4. Calculated penetration distance and maximum pitch during ship ramming

Ice thickness (Input thrust)	Ram. No.	Arrival point [m]	Penetration distance [m]	Maximum Pitch [deg.]
3.0 m (35 kN/m)	1	80.15		1.16
	2	144.39	61.24	2.01
	3	135.58	54.74	2.23
	Average		57.99	1.80
3.5 m (35 kN/m)	1	42.71		4.21
	2	75.96	33.25	4.07
	3	117.89	41.93	4.11
	4	161.37	43.48	3.96
	Average		39.55	4.09
4.0 m (40 kN/m)	1	22.82		5.12
	2	45.11	22.30	4.27
	3	67.57	22.46	3.90
	4	90.89	23.32	2.16
	5	114.03	23.14	4.91
	Average		22.80	4.07
4.5 m (40 kN/m)	1	22.69		5.10
	2	46.10	23.41	3.54
	3	48.22	2.12	5.04
	4	71.06	22.84	3.43
	5	74.07	3.01	4.85
	Average		12.84	4.39
5.0 m (45 kN/m)	1	22.64		5.11
	2	24.70	2.06	4.70
	3	26.74	2.04	4.74
	4	28.75	2.01	4.74
	5	30.89	2.14	4.68
	6	46.77	15.88	2.55
	7	58.56	11.79	4.72
	8	60.48	1.96	4.74
	Average		5.41	4.50

REFERENCES

Araoka. K., and Maeno. N., 1978. Measurements of Restitution Coefficients of Ice, *Low Temperature Science*, A, 36, pp.55-65 (in Japanese).

Baraff, D., 1997. Rigid Body Simulation I, II, *Siggraph 97 Course notes*.

Blanchet, B., Kivisid, H. R. & Grinstead, J., 1990. Equations for local ice energy dissipations during ship ramming, *Cold Region Science and Technology*, 18, pp.101-115.

Daley, C. G. & Riska, K., 1990. Review of Ship–ice Interaction Mechanics. *Report from Finnish–Canadian Joint Research Project No. 5 "Ship Interaction with Actual Ice Conditions" Interim Report on Task 1A. Helsinki*, Finland: Helsinki University of Technology, pp.19-35.

Dimgliana, J. and O'Sullivan, C., 2000. Graceful degradation of collision handling in physically based animation, *Computer Graphics Forum*, 19(3), pp. 239–248.

Kishi, S. & Kawashima, Y., 1997. Ramming Performance of the Patrol Icebreaker "PM TESHIO" in Full Scale and Model Scale. *Proceedings of OMAE/POAC Joint Conference*, 4, pp.233-238.

Nozawa, K., 2006. *Sea ice Engineering*. Seizando-Shoten Publishing Co. Ltd. Japan (in Japanese).

Ringsberg, J. W., Broman, M., & Nordqvist, P., 2014. Development of a Model for Global Response of Ship Hull during Ramming of Heavy Ice Features. *Proceedings of the ASME 2014 33rd International Conference on OMAE*, OMAE2014-23186.

Sawamura J., Riska K., Moan T., 2009. Numerical Simulation of Breaking Pattern in Level Ice at Ship's Bow, *Proceedings of 19th International Offshore and Polar Engineering Conference*, pp. 600–607.

Sawamura, J et al., 2017. Simulation of Ice Force and Breaking Pattern for Icebreaking Ship in Level Ice, *Proc. ASME 2017 36th International Conference on Ocean and Arctic Engineering*. CD-ROM, OMAE2017-61583

Sawamura J., Yamaguchi H., Ushio S., and Yamauch Y., 2020. Calculation of penetration distance during ship ramming in multi-year ice, *Okhotsk Sea and Polar Oceans Research*, 4, pp.10-17.

Vaughan H., 1986. Flexural Response of Ice-Breaking Ships to Impact Loads, *RINA Transactions*, 7, 259-267.

Yamauchi, Y., Mizuno, S., & Tsukuda, H., 2011. The icebreaking performance of SHIRASE in the maiden Antarctic voyage. *Proceeding of the 21st International Offshore and Polar Engineering Conference*, pp.1093-1099.